Validity of RHEED specular intensity measurements for structural studies of liquid metal surfaces: applications to liquid In and Sn

1991 J. Phys.: Condens. Matter 3 2769

(http://iopscience.iop.org/0953-8984/3/16/016)

J. Phys.: Condens. Matter 3 (1991) 2769–2785. Printed in the UK

Validity of RHEED specular intensity measurements for structural studies of liquid metal surfaces: applications to liquid In and Sn

M Hasegawa† and T Ichikawa‡

† Department of Mathematics, Faculty of Engineering, Iwate University, Morioka 020, Japan

‡ Department of Physics, School of Science and Technology, Meiji University, Kawasaki 214, Japan

Received 3 July 1990, in final form 18 December 1990

Abstract. We propose a method of analysing the glancing angle dependence of the RHEED (reflection high-energy electron diffraction) specular intensity $I(\theta)$ from liquid metal surfaces and apply it to liquid In and Sn, for which preliminary RHEED experiments have recently been performed. We use two models to derive a scattering potential that is supposed to cause the specular reflection of fast electrons. Calculations of $I(\theta)$ based on these models reveal that the tail behaviour of the scattering potential on the vapour side essentially determines the characteristics of $I(\theta)$ in the range of small glancing angle θ. The comparisons of these calculations with experiments suggest that the scattering potential in the liquid–vapour transition zone of liquid In results from neutral atoms, while the scattering potential due to ions and extended conduction electrons is plausible for liquid Sn even in the surface region. It is concluded from the present analyses that we need accurate experimental data for $I(\theta)$ in a wider range of θ to determine the full behaviour of the surface density profiles of liquid metals.

1. Introduction

Over the last two decades increasing attention has been paid to the microscopic theory of liquid metal surfaces, and various types of theories have been developed [1]. These theories are generally successful in predicting the surface tension of liquid simple metals such as the alkali metals. However, all these theories are too crude or much too complicated to provide a unified description for the surface tension and surface structures of liquid metals. Rice and coworkers have primarily been concerned with the density profiles in the liquid–vapour transition zone and performed Monte Carlo (MC) simulations for liquid Na, Cs and Hg [2–4]. The atomic density profiles obtained in these studies exhibit oscillatory or stratified structures on the scale of the interatomic distance. Improved MC simulations for liquid Na [5] and analyses of x-ray reflectance experiments on liquid Cs and Hg [6–8] also support the existence of such a structure in the density profiles.

We wish to make some comments on the theoretical and numerical simulation studies of liquid metal surfaces. The most serious difficulty in these studies is the calculation of the effective Hamiltonian, which determines the energetics of the atoms (or ions) in the

0953-8984/91/162769 + 17 $03.50

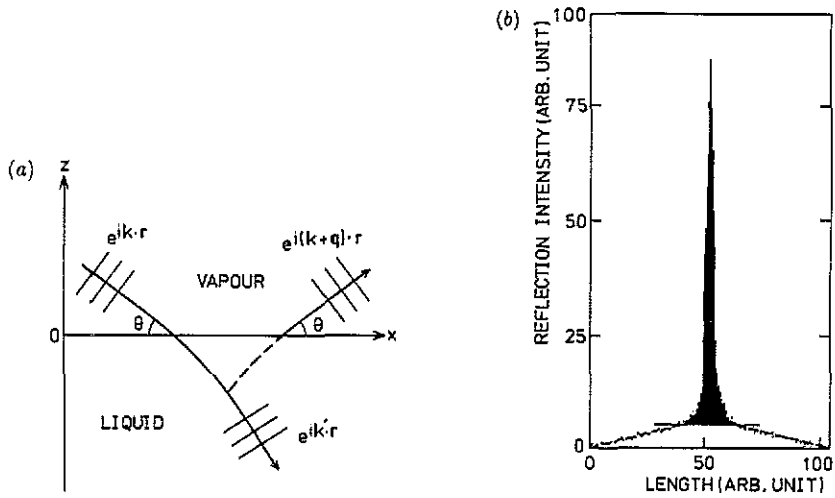

Figure 1. (*a*) Schematic illustration of the specular reflection of fast electrons (or x-rays) from a liquid metal surface. (*b*) A typical example of the RHEED reflection intensity obtained by integrating the two-dimensional intensity detected on the fluorescent plate (placed perpendicular to the specularly reflected electron beam) in one direction. The shaded area represents the specular intensity.

highly inhomogeneous liquid–vapour transition zone [1, 2]. The achievement of self-consistency between the ionic and electronic densities is also a difficult problem [4]. These difficulties are quite serious in the theoretical studies and, as we noted above, no microscopic theory has been successful in predicting surface density profiles consistent with the results of the x-ray reflectance experiments. It seems that numerical simulations suffer much less from these difficulties, as they actually produced surface density profiles consistent with the x-ray results [2–5].

In the present work we are concerned with reflection high-energy electron diffraction (RHEED), which could be another useful experimental method complementary to x-ray reflectance experiments. Suppose that a plane wave (x-ray or electron beam) is incident on to the surface of a liquid metal and reflected. We take the z axis along the direction perpendicular to the liquid surface and let θ be the glancing angle of the incident wave with wavevector $\boldsymbol{k}$ (see figure 1(*a*)). We take the axis of coordinates such that $\boldsymbol{k}$ lies in the xz plane, so $\boldsymbol{k} = (k_x, 0, k_z)$ with $k_x = k\cos\theta$ and $k_z = -k\sin\theta$, and the asymptotic form of the specularly reflected wave is represented by the plane wave with wavevector $\boldsymbol{k} + \boldsymbol{q}$, where $\boldsymbol{q} = (0, 0, q)$ with $q = 2k\sin\theta$. If the atomic density profile exhibits any oscillatory or stratified structure near the surface, we may expect an anomalous bump in the specular reflection intensity $I(\theta)$ around the glancing angle θ, which satisfies the condition $2\pi/q = l$ or $\lambda/2\sin\theta = l$, where l is the characteristic length of the structure in the density profile and $\lambda = 2\pi/k$ is the wavelength of the incident wave. The magnitude of l may be of order of the interatomic distance in bulk liquids and so $l \simeq 3$ Å for liquid In and Sn, with which we are concerned in the present work. Therefore, if we use a typical x-ray source, say the Cr K_α line with $\lambda = 2.29$ Å, in the x-ray reflectance experiments on liquid In or Sn, the glancing angle θ that satisfies the above condition is about 400 mrad. The x-ray reflectance data are actually available in the range of much smaller θ, i.e. $\theta \leqslant 40$ mrad. In other words, the characteristic length that can be directly probed in the

x-ray reflectance experiments is about one order of magnitude larger than l, although analyses of such experiments have successfully been made [6–8].

In RHEED, the reflectivity could be obtainable at glancing angles θ amounting to much larger momentum transfers q and so covering the characteristic length l. In fact, for $E = \hbar^2k^2/2m = 20$ keV, which is the energy of the electron beam employed in the recent RHEED experiments, the value of θ satisfying the condition $2\pi/q = l = 3$ Å is about 15 mrad and in the range where experimental $I(\theta)$ is available. This analysis suggests that RHEED provides a useful method, at least in principle, for studying the structures of liquid metal surfaces. If we take into account the refraction effect, which we ignored in the above analysis, the momentum transfer q' inside the surface is larger than q and the corresponding θ' is smaller than the above value (see figure 1(a)). We also note that an electron beam couples much more strongly with materials and hence is a more surface-sensitive probe than an x-ray beam. This fact is also gratifying unless the coupling is too strong to prevent the electron beam penetrating liquid metals to a reasonable depth. The actual situation concerning these points will be clarified in the present paper.

Based on the above considerations, one of the authors (TI) has performed preliminary RHEED experiments on liquid In and Sn. These experiments have not yet been successful in the measurement of the reflectivity over a sufficiently wide range of θ but provided a remarkable preliminary result: the reflectivity of liquid Sn decreases much faster on increasing θ than that of liquid In, implying that the surface structures of these liquid metals are quite different from each other. This is an unexpected finding, because many other properties such as the surface tension and viscosity of these liquid metals are quite similar to each other.

A solution to the scattering problem for fast electrons in liquid metals is a prerequisite in the analyses of the RHEED experiments. Such a scattering problem is difficult to solve and some simplifying approximations are inevitable to make the problem tractable. The purpose of the present work is to establish a theoretical method which, although approximate, can be applied to the analyses of RHEED specular intensity data and to confirm the validity of the RHEED experiments in the structural studies of liquid metal surfaces. The results of the present study are expected to provide a useful guideline for further extensive RHEED experiments. A preliminary account of the present work can be found elsewhere [9].

The organization of this paper is as follows. In section 2, we introduce the method used to calculate the RHEED specular intensities $I(\theta)$ for liquid metals, with special emphasis on the approximate nature inherent in the method. In section 3, we apply our method to liquid In and Sn and investigate how $I(\theta)$ is related to the atomic density profiles. The results of calculations for $I(\theta)$ are also compared with the preliminary experiments, with particular interest in the origin of the difference between these two metals implied by the observed $I(\theta)$. The final section is devoted to a summary and conclusions.

2. Specular reflection of fast electrons from liquid metal surfaces

Fast electrons incident on a liquid metal surface suffer scattering, and the scattered waves can be classified into elastic and inelastic waves produced by elastic and inelastic scattering, respectively, although the two are not independent but are coupled to each other. We are concerned with the particular elastic wave giving rise to specular reflection,

for which a structural inhomogeneity along the direction perpendicular to the surface is responsible. The reflection intensities due to the other scattered waves including inelastic waves provide a diffuse background of the specular intensity. Experimentally, such a specular intensity can be obtained by subtracting the background from the total intensity in an appropriate manner as demonstrated in figure 1(*b*). In the analyses of the specular intensity obtained in this way, one must be able to calculate, for a given surface structure, the amplitude of the elastic wave giving rise to the specular reflection. One of the most difficult problems in such calculations is how to treat the effect of inelastic scattering on the particular elastic wave.

We note that, with the inelastic scattering taken into account, the amplitude of any elastic wave would be lower than otherwise, and in this sense the inelastic scattering may be treated as effectively causing the 'absorption' of elastic waves. In fact, such a treatment of inelastic scattering in perfect crystals has been established and the scattering of fast electrons can be described by the complex periodic potential [10, 11]

$$V(\boldsymbol{r}) = \sum_{\boldsymbol{G}} [V_{\mathrm{R}}(\boldsymbol{G}) + \mathrm{i}V_{\mathrm{I}}(\boldsymbol{G})] \exp(\mathrm{i}\boldsymbol{G}\cdot\boldsymbol{r}) \tag{1}$$

where $\boldsymbol{G}$ is the reciprocal lattice vector. The real part $V_{\mathrm{R}}(\boldsymbol{G})$ in equation (1) is the usual structure potential consisting of the electrostatic potentials of the crystal atoms. In the absence of inelastic scattering, $V_{\mathrm{R}}(\boldsymbol{G})$ determines the power intensity of the diffraction spot associated with $\boldsymbol{G}$. On the other hand, the imaginary part $V_{\mathrm{I}}(\boldsymbol{G})$ accounts for the inelastic scattering and represents the 'absorption' effect on that diffraction spot. The most important mechanisms of inelastic scattering are the excitations of phonons, atomic electrons and plasmons (in the case of metals). The inelastic scattering mechanisms in liquid metals are similar to those in crystals, although phonons in liquids are not so well defined as in crystals. In spite of this similarity, the above treatment of inelastic scattering cannot be applied to liquid metals in which no translational symmetry exists and the wavevectors of scattered waves are continuously distributed. We also note that, while we are primarily concerned with the surface, no such effect is included in the above treatment. Nevertheless, it may be useful to estimate the 'absorption' effect due to the inelastic scattering in the case of crystals.

In the above treatment of the scattering problem, the effect of inelastic scattering can be described in terms of the appropriately defined absorption coefficients. The significance of such absorption effects on the diffraction spots depends on the size and geometry (i.e. crystal orientation relative to the incident electron beam) of crystals. We used the tables given by Radi [11] to estimate the absorption coefficient $\mu_0 = -(2m/\hbar^2 k)V_{\mathrm{I}}(0)$, which is appropriate for electrons transmitted through crystals without being scattered and may be used for nearly-forward scattering. In these tables, the values of $V_{\mathrm{I}}(\boldsymbol{G})$ are given for the external electrons with $E = 100$ keV and we have to multiply these values by the appropriate conversion factor to obtain the values in our case ($E = 20$ keV). The value of μ_0 obtained in this way is about 0.030 Å^{-1} for both In and Sn crystals and not very large. (This value of μ_0 was estimated from those for other metals, since In and Sn are not contained in the tables of [11].) We note that phonon excitations dominate $V_{\mathrm{I}}(\boldsymbol{G})$ with $\boldsymbol{G} \neq 0$ but contribute very little to $V_{\mathrm{I}}(0)$. Therefore, μ_0 is insensitive to the temperature and the above value of μ_0 for crystals may also be used for liquid In and Sn. As we have mentioned in the above, the significance of inelastic scattering is not determined only by the 'absorption' coefficients but also depends on the experimental situation. In fact, the absorption effect may be insignificant in the case of RHEED, as we discuss immediately below.

In RHEED experiments for liquid metals, in which fast electrons are incident with small glancing angles, the wave field is predominantly distributed in the surface region. The inelastic scattering in such a situation is more restrictive than in the bulk and the absorption coefficient μ_0 would be much reduced compared to that estimated in the above. Furthermore, though not justified *a priori* but confirmed in our analyses, the scattering that occurs in the liquid–vapour transition zone dominates the specular reflection intensity and the electrons involved in such scattering travel only a short distance through the liquid metals. All these characteristic features of RHEED suggest that we may safely ignore the effect of inelastic scattering in the analyses of the experimental data. We followed these arguments and entirely ignored the effect of inelastic scattering in the present work. A more complete justification for ignoring inelastic scattering constitutes an important theoretical work and is outside the scope of the present work.

In the above basic approximation, we may consider that external electrons are scattered by the structure potential $V(r)$ composed of the electrostatic potentials due to atoms (or ions and conduction electrons). In the calculations of the RHEED specular reflection intensities, the Schrödinger equation in our scattering problem is conveniently written as

$$\left(-\frac{\hbar^2\nabla^2}{2m} + V_s(z) + \Delta V(r) \right) \Psi(r) = E\Psi(r) \tag{2}$$

where $E = \hbar^2k^2/2m$ is the energy of an incident electron with wavevector k, $V_s(z) = \langle V(r) \rangle$ is a smoothed or averaged potential obtained by smearing $V(r)$ in the plane parallel to the surface and $\Delta V(r) = V(r) - V_s(z)$. The wavefunction $\Psi(r)$ in equation (2) is subject to an appropriate asymptotic condition. $V_s(z)$ will be called a *surface potential* hereafter. The specular reflection of incident electrons is essentially determined by $V_s(z)$, while $\Delta V(r)$ may be treated, though not rigorously, as giving rise to the non-specular reflection as well as causing the 'absorption' of the incident, refracted and specularly reflected waves through multiple scattering. In fact, any electron that is scattered and has no chance of returning is lost from the original wave and, in this sense, multiple scattering effectively causes the 'absorption' of any wave.

The above 'absorption' effect due to multiple scattering is similar to that due to inelastic scattering and its significance can also be estimated, though approximately, in terms of the absorption coefficient. If we assume that the atoms in liquids can be treated as independent scatterers, the absorption coefficient due to multiple scattering is given by $\mu_M = \rho\sigma_{atom}$, where ρ is the number density of atoms and σ_{atom} is the scattering cross section of a single atom. In the Born approximation, σ_{atom} is given by

$$\sigma_{atom} = \frac{m}{4\pi\hbar^2 E} \int_0^{2k} |v_{atom}(q)|^2 q \, dq \tag{3}$$

where $v_{atom}(q)$ is the atomic form factor, i.e. the Fourier transform of the atomic potential $v_{atom}(r)$ (see equation (8)). For the In atom, we obtained $\sigma_{atom} = 0.67$ Å^2 for $E = 20$ keV and so $\mu_M = 0.025$ Å^{-1} in the bulk liquid. This value of μ_M is comparable to the absorption coefficient μ_0 due to inelastic scattering. In the liquid-vapour transition zone, where the atomic density is much lower than the bulk density, the magnitude of μ_M is much smaller than the above value. Therefore, following the arguments given for the effect of inelastic scattering, we may also ignore the effect of multiple scattering. This approximation may be viewed as an *effective refractive index model* without dissipation.

In the above approximation ($\Delta V(r) = 0$), the wavefunction $\Psi(r)$ in equation (2) is expressed as $\Psi(r) = \exp(ik_x x)\exp(ik_y y)w(z)$, where $k_y = 0$ in our case (see figure 1(*a*)), and the problem is reduced to the one-dimensional scattering problem represented by the Schrödinger equation

$$-\frac{\hbar^2}{2m}\frac{d^2w(z)}{dz^2} + V_s(z)w(z) = \frac{\hbar^2 k_z^2}{2m}w(z). \tag{4}$$

In equation (4), $k_z = -k\sin\theta$ as before and the wavefunction $w(z)$ is subject to the asymptotic condition given by

$$w(z) = \begin{cases} a\exp(ik_z z) + b\exp(-ik_z z) & (z \to \infty) \\ \exp(ik_z' z) & (z \to -\infty) \end{cases} \tag{5}$$

where

$$k_z' = k_z[1 - V_s(-\infty)/E\sin^2\theta]^{1/2}. \tag{6}$$

Once $V_s(z)$ is given, we can determine the constants a and b in equation (5) by solving the above Schrödinger equation (equation (4)) numerically by the standard method (e.g. Runge–Kutta–Gill method). Then, the specular intensity (reflectivity) is given by $I(\theta) = |b/a|^2$.

2.1. Model I

In the present work we used two models to calculate the structure potential $V(r)$ felt by an external electron. In the first model (which we call model I hereafter), $V(r)$ is given by the superposition of the atomic potentials:

$$V(r) = \sum_i v_{\text{atom}}(|r - r_i|). \tag{7}$$

In equation (7), r_i represents the position of the ith atom and v_{atom} is the atomic potential given by

$$\begin{aligned} v_{\text{atom}}(s) &= -\frac{Z_N e^2}{s} + \int dt \frac{n_{\text{atom}}(t)e^2}{|s-t|} \\ &= -\frac{Z_N e^2}{s} + \frac{1}{s}\int_0^s \sigma(t)\,dt + \int_s^\infty \frac{\sigma(t)}{t}\,dt \end{aligned} \tag{8}$$

where Z_N is the atomic number, $n_{\text{atom}}(t)$ is the electron density in each atom and $\sigma(t) = 4\pi t^2 n_{\text{atom}}(t)e^2$. The Fourier transform of $v_{\text{atom}}(r)$ is the atomic form factor $v_{\text{atom}}(q)$ in equation (3). The above treatment of the structure potential has been common practice in the analyses of electron diffraction experiments [11]. The exchange and correlation effects between the external and metallic electrons may be ignored for high-energy electrons in RHEED experiments.

The above model may be called a neutral atom model and is clearly not adequate in bulk metals. The valence electrons should be treated more properly as extended conduction electrons, at least in bulk metals, and we actually make such a treatment in our second model. However, for a metal consisting of heavy atoms, the electrostatic potential due to the core electrons dominates the electronic contribution to $V(r)$ and any difference arising from the different treatments of the valence electrons could be

insignificant in bulk metals. We will come back to this problem when we apply our models to the analyses of RHEED experiments.

In our *effective refractive index model*, the surface potential $V_s(z)$ may most naturally be given by the thermal average of $V(\boldsymbol{r})$:

$$V_s(z) = \left\langle \sum_i v_{\text{atom}}(|\boldsymbol{r} - \boldsymbol{r}_i|) \right\rangle = \int d\boldsymbol{r}' v_{\text{atom}}(|\boldsymbol{r} - \boldsymbol{r}'|) \left\langle \sum_i \delta(\boldsymbol{r}' - \boldsymbol{r}_i) \right\rangle$$

$$= \int d\boldsymbol{r}' \, v_{\text{atom}}(|\boldsymbol{r} - \boldsymbol{r}'|)\rho(z') \tag{9}$$

where $\langle \ldots \rangle$ represents the thermal average and $\rho(\boldsymbol{r}) = \langle \sum_i \delta(\boldsymbol{r} - \boldsymbol{r}_i) \rangle$ is the atomic one-body distribution function (i.e. atomic number density) [12], which is a function of only z for a planar surface. Equation (9) can be reduced to

$$V_s(z) = 2\pi \int_{-\infty}^{\infty} dz' \, \rho(z' + z) \int_{|z'|}^{\infty} d\boldsymbol{r} \, r v_{\text{atom}}(r). \tag{10}$$

Equation (9) or (10) relates $V_s(z)$ to $\rho(z)$ in our effective refractive index model. A similar approach has been adopted implicitly in the analyses of x-ray reflectance experiments [6–8].

2.2. *Model II*

As we have discussed in the preceding subsection, the valence electrons should be treated as extended conduction electrons, at least in bulk metals. In such a treatment (which we call model II hereafter), $V(\boldsymbol{r})$ is given by

$$V(\boldsymbol{r}) = \sum_i v_{\text{ion}}(|\boldsymbol{r} - \boldsymbol{r}_i|) + \int d\boldsymbol{r}' \frac{n(\boldsymbol{r}')e^2}{|\boldsymbol{r} - \boldsymbol{r}'|} \tag{11}$$

where $v_{\text{ion}}(r)$ is the electrostatic potential due to the nucleus and core electrons in each ion and $n(\boldsymbol{r})$ is the number density of the extended conduction electrons. In order to avoid the difficulty associated with the long-range Coulombic interactions, equation (11) can conveniently be rewritten as

$$V(\boldsymbol{r}) = \sum_i v'_{\text{ion}}(|\boldsymbol{r} - \boldsymbol{r}_i|) + \varphi_M(\boldsymbol{r}) + \varphi_{es}(\boldsymbol{r}) \tag{12}$$

where

$$v'_{\text{ion}}(s) = v_{\text{ion}}(s) + Ze^2/s \tag{13}$$

$$\varphi_M(\boldsymbol{r}) = \int d\boldsymbol{r}' \frac{Ze^2\rho_0(\boldsymbol{r}')}{|\boldsymbol{r} - \boldsymbol{r}'|} - \sum_i \frac{Ze^2}{|\boldsymbol{r} - \boldsymbol{r}_i|} \tag{14}$$

and

$$\varphi_{es}(\boldsymbol{r}) = \int d\boldsymbol{r}' \frac{e^2[n(\boldsymbol{r}') - Z\rho_0(\boldsymbol{r}')]}{|\boldsymbol{r} - \boldsymbol{r}'|}. \tag{15}$$

In the above equations, Z is the valence of the ion and $\rho_0(\boldsymbol{r})$ is an (assumed) ionic number density. We note that in the above expression for $V(\boldsymbol{r})$ we added and subtracted the terms containing Z and $\rho_0(\boldsymbol{r})$ and, although $\rho_0(\boldsymbol{r})$ may be chosen arbitrarily, it is most conveniently chosen to be the true one $\rho(z)$ as we actually do in the following.

We must be careful in the treatment of $\varphi_M(r)$, which we call the Madelung potential, since its thermal average $\langle\varphi_M(r)\rangle$ vanishes. In the Wigner–Seitz (WS) approximation, which is useful in bulk metals, φ_M is given by

$$\varphi_M(r) = 2\pi\rho_b Ze^2(R_s^2 - \tfrac{1}{3}r^2) - Ze^2/r$$

where R_s is the atomic (or WS) sphere radius defined by $(4\pi/3)R_s^3 = 1/\rho_b$, ρ_b being the atomic number density of a (bulk) metal, and r is the distance from the ion in each atomic sphere. The average value of $\varphi_M(r)$ in the atomic sphere is then given by [11]

$$\bar{\varphi}_M = -\tfrac{3}{10}Ze^2/R_s$$

and this result may be used in bulk metals. In order to calculate φ_M in inhomogeneous liquid metals, we employed an intuitive approximation that may be viewed as a local density approximation:

$$\varphi_M(z) = -\tfrac{3}{10}Ze^2/R_s(z) \tag{16}$$

where $R_s(z)$ is the atomic sphere radius defined by the local density $\rho(z)$: $(4\pi/3)R_s(z)^3 = 1/\rho(z)$.

For a planar surface, the electron density $n(r)$ is also a function of only z if the electron–ion interaction is taken into account to first order in the perturbation calculations [1, 13, 14]. In this approximation, the electrostatic potential φ_{es} given by equation (15) can easily be calculated from the Poisson equation (rather than directly from equation (15)) once $\rho(z)$ and the corresponding $n(z)$ are given. The result is given by

$$\varphi_{es}(z) = -4\pi e^2 \int_z^\infty dz' \int_{z'}^\infty dz'' \,[n(z'') - Z\rho(z'')] \tag{17}$$

with $\varphi_{es}(\infty) = 0$. The method of calculating $n(z)$ is discussed below.

Then, the surface potential $V_s(z)$ in model II corresponding to that in equation (9) is given by

$$V_s(z) = \int dr' v'_{ion}(|r - r'|)\rho(z') + \varphi_M(z) + \varphi_{es}(z) \tag{18}$$

where the first term on the RHS, which we denote $\varphi_0(z)$ in table 1, is the thermal average of the first term on the RHS of equation (12), and $\varphi_M(z)$ and $\varphi_{es}(z)$ are given by equations (16) and (17) respectively.

The remaining problem in model II is the calculation of the electron density profile $n(z)$ for a given $\rho(z)$. As we have mentioned above, in order to calculate $n(z)$ we employed first-order perturbation theory, making use of a simple empty-core model potential [15]. In this approximation, together with the local density approximation (LDA) for the exchange and correlation energies of an inhomogeneous electron jellium, we could follow Lang and Kohn and calculate $n(z)$ by solving the Kohn–Sham equation applied to the surface [16]. In the present work, however, we employed a variational method, which is much simpler and easily tractable [1, 13, 14].

In our variational calculations, we assumed that the Gibbs dividing surfaces of both electrons and ions are located at $z = 0$ and used a parametrized $n(z)$ of the form

$$n(z) = \begin{cases} n_b[1 - A\exp(\alpha_1 z)\cos(\gamma z)] & (z < 0) \\ n_b(1 - A)\exp(-\alpha_2 z) & (z > 0) \end{cases} \tag{19}$$

where n_b is the bulk density. Two of the four parameters A, α_1, α_2 and γ in equation

(19) can be eliminated by the requirements that $dn(z)/dz$ is continuous at $z = 0$ and the Gibbs dividing surface is located at $z = 0$, i.e.

$$\int_{-\infty}^{0} [n(z) - n_b]\,dz + \int_{0}^{\infty} n(z)\,dz = 0. \tag{20}$$

The remaining parameters are determined so as to minimize, for a given ionic density $\rho(z)$, the electronic contributions to the surface energy. In our calculations, we used the LDA for the exchange and correlation energies and the density-gradient expansion for the kinetic energy of an inhomogeneous electron jellium. In the density-gradient expansion we included up to second gradient terms (fourth order in the gradient of $n(z)$). The details of the computational procedures are given elsewhere [1, 13, 14]. We have confirmed that the surface properties of the electron jellium calculated in this way are in reasonable agreement with the corresponding results of Lang and Kohn [16] in the range of metallic densities.

3. Applications to liquid In and Sn

Preliminary RHEED experiments were performed for liquid In and Sn just above their melting points. These metals were chosen for practical reasons such as their low melting temperatures and low vapour pressures. The energy E of the electron beam used in these experiments was 20 keV and the RHEED specular intensities $I(\theta)$ were measured for varying glancing angle θ. We also use this value of E throughout the following analyses.

We performed atomic structure calculations for a neutral atom to calculate the atomic potential $v_{atom}(r)$ in equation (8). We also used a neutral atom rather than a free ion to calculate the ionic core states used in the calculations of $v_{ion}(r)$ in equation (11), because the ionic core states calculated in this manner should be more appropriate in solids or liquids. The parameters and inner values of the surface potentials $V_s(z)$ of liquid In and Sn are summarized in table 1.

3.1. General aspects

We first investigated general aspects of the interrelation between the surface potentials $V_s(z)$ and the RHEED specular intensities $I(\theta)$. For this purpose, we used a parametrized density profile of the form

$$\rho(z) = \begin{cases} \rho_b[1 - B\exp(\beta_1 z)\cos(\delta z)] & (z < 0) \\ \rho_b(1 - B)\exp(-\beta_2 z) & (z > 0). \end{cases} \tag{21}$$

Two of the four parameters B, β_1, β_2 and δ can be eliminated by the same requirements as those imposed on $n(z)$ given by equation (19). The above form of $\rho(z)$ has frequently been used in the theoretical studies of liquid metal surfaces [1, 14].

We considered both monotonic and oscillatory density profiles in our analyses. Monotonic profiles are obtained if we set $\delta = 0$ in equation (21) and in this case $1/\beta_1$ $(= 1/\beta_2)$ represents the degree of surface width. An oscillatory or stratified structure in $\rho(z)$, if any, is a manifestation of the correlation between atoms and a steep confining potential (for atoms in liquids) formed at the surface (see figure 2(*b*)). Such an oscillation in $\rho(z)$ is essentially the same as that found in the radial distribution function $g(r)$ in bulk liquids. In the previous work [9], we used a value of $\delta R_s = 3.8$, which produces an

Table 1. Parameters and inner values of the calculated surface potentials of liquid In and Sn at their melting points T_m. Here r_c is the empty-core radius of the model potential [15] used in model II and $\varphi_0(z)$ represents the first term on the RHS of equation (18). The inner potential $V_s(-\infty)$ and its component parts are given in units of eV. The values of $\varphi_{es}(-\infty)$ and $V_s(-\infty)$ in model II (equation (18)), which are not sensitive to the ion density profile $\rho(z)$, are those calculated for the $\rho(z)$ given by equation (21) with $\delta R_s = 4.2$ and $\beta_1 R_s = 0.7$ (curve B in figure 2(*a*)).

						Model I	Model II			
Metal	Z_N	Z	T_m (K)	R_s (au)	r_c (au)	$V_s(-\infty)$	$\varphi_0(-\infty)$	$\varphi_M(-\infty)$	$\varphi_{es}(-\infty)$	$V_s(-\infty)$
In	49	3	430	3.52	1.32	−18.61	−8.36	−6.95	−7.98	−23.29
Sn	50	4	505	3.57	1.30	−18.62	−7.09	−9.14	−9.96	−26.19

oscillation in $\rho(z)$ similar to that in $g(r)$. However, we find that a slightly larger value of δ is more plausible in accordance with the results of MC simulations for Na and Cs [2–5] and with the analyses of the x-ray reflectance experiments [8]. Therefore, we used a value of $\delta R_s = 4.2$ for oscillatory $\rho(z)$ in the present analyses, although the difference arising from this change (about 10%) in the value of δ is minimal. Other values of δ (for oscillatory $\rho(z)$) much different from the above values are not completely precluded but are difficult to interpret on a physical basis.

Figure 2(*a*) shows some typical examples of the atomic (or ionic) density profiles $\rho(z)$ given by equation (21) and the corresponding electron density profiles $n(z)$ (equation (19)) obtained for liquid In, the latter of which is relevant in model II. The surface potentials $V_s(z)$ and RHEED specular intensities $I(\theta)$ calculated for these $\rho(z)$ in the models are shown in figures 2(*b*) and (*c*) respectively. The main points of these results are as in the following.

(i) We find in figure 2(*a*) that the electron density $n(z)$ in model II shows a large relaxation at the surface and is not sensitive to the details of the ionic density profiles $\rho(z)$. This result can be understood by the important role played by the kinetic energy of the conduction electrons, which favour smooth densities, in determining the density in inhomogeneous systems [16]. The electrostatic dipole potential $\varphi_{es}(z)$ in model II dominates the tail part of $V_s(z)$ on the vapour (vacuum) side because of the large relaxation of $n(z)$ at the surface and the resulting $V_s(z)$ in model II shows a slow variation in that region compared to that in model I. The values of $V_s(-\infty)$ (i.e. the depth of $V_s(z)$ in the bulk) in the two models are also somewhat different from each other (see figure 2(*b*) and table 1) and, with the exception of this difference, the two models are quite similar to each other in the bulk side. As we will discuss below, the RHEED specular intensity $I(\theta)$ is not sensitive to the depth of $V_s(z)$ and therefore the important difference between the two models may be characterized by the different behaviours of $V_s(z)$ on the vapour side.

(ii) In the range of small glancing angles ($\theta \leq 8$ mrad), the RHEED specular intensities $I(\theta)$ obtained in model II decrease much faster on increasing θ than those in model I (see figure 2(*c*)). These results can be explained by the fact that the tail part of $V_s(z)$ on the vapour side essentially determines $I(\theta)$ in the range of small θ: the more slowly that part of $V_s(z)$ varies, the more rapidly $I(\theta)$ decreases on increasing θ in that range, almost irrespective of the behaviours of $V_s(z)$ on the bulk side. The steep rises of $V_s(z)$ on crossing the liquid–vapour transition zone begin to influence $I(\theta)$ at $\theta \simeq 8$ mrad and the

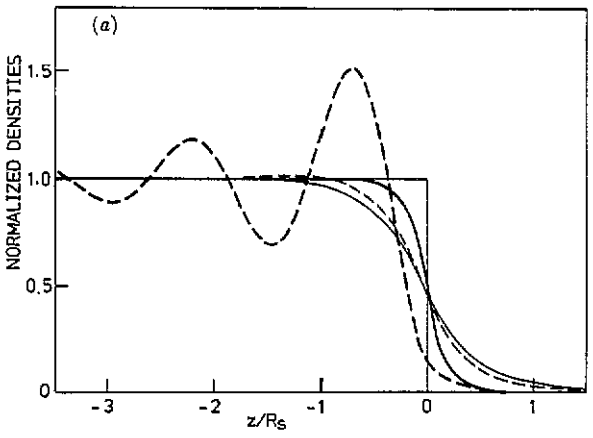

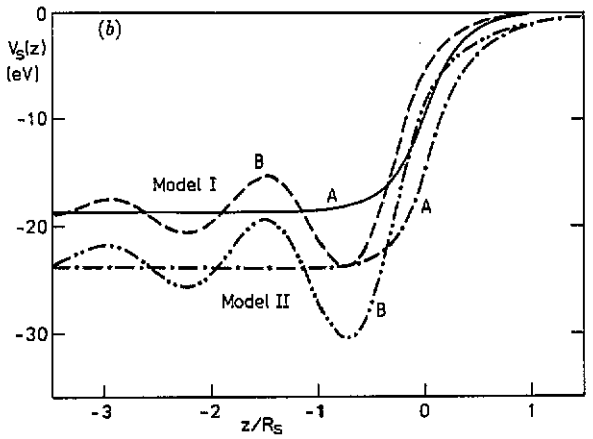

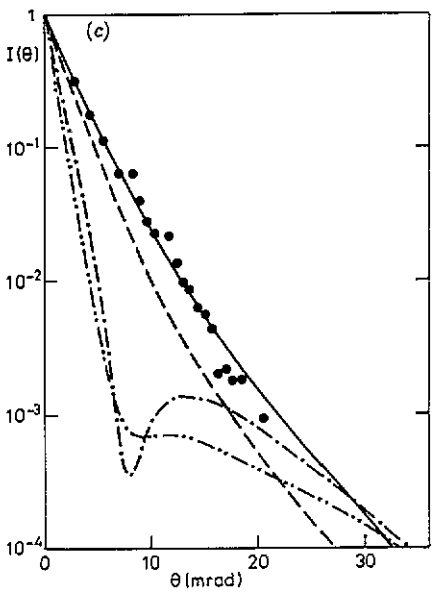

Figure 2. (*a*) Typical examples of the atomic (or ionic) density profiles $\rho(z)$ given by equation (21): A (full curve), $\delta = 0$ and $\beta_1 R_s = 6.5$; B (broken curve), $\delta R_s = 4.2$ and $\beta_1 R_s = 0.7$. Thin curves (full and broken) are the corresponding electron density $n(z)$ (equation (19)) in model II. The step density profile is also shown in this figure for comparison. (*b*) Surface potentials $V_s(z)$ in two models (equations (9) and (18)). Curves A and B in each model are those calculated respectively for the atomic (or ionic) density profiles A and B in (*a*). (*c*) Comparisons of the calculated (curves) and experimental (full circles) RHEED specular intensities $I(\theta)$ for liquid In. Each curve corresponds to that in (*b*) and the experimental data are normalized such that the smooth extrapolation of $I(\theta)$ to $\theta = 0$ is unity.

bumps around $\theta = 15$ mrad found in $I(\theta)$ of model II can be ascribed to that behaviour of $V_s(z)$. In contrast with this, $I(\theta)$ in model I shows no such behaviour but happens to decrease monotonically on increasing θ. Such a structureless $I(\theta)$ can be explained as follows: the steep rise and tail behaviour of $V_s(z)$ in model I are roughly characterized by a single-exponential function reflecting such a variation of $\rho(z)$ for $z > 0$ (see equation (21)).

(iii) As we have discussed in section 1, one would have expected an anomalous bump in $I(\theta)$ for an oscillatory $\rho(z)$. Contrary to this expectation, $I(\theta)$ exhibits no such anomaly that can be ascribed to the oscillation of $\rho(z)$, as is clear from the results of $I(\theta)$ in model I. One reason for this is that the scattering that occurs inside the surface contributes very little to $I(\theta)$ in the range of small θ and, as we have discussed in the above, $I(\theta)$ is essentially determined by the scattering that occurs on the vapour side. Another reason is discussed below.

(iv) In spite of the above unfavourable feature of RHEED, it may be useful to see more closely the present situation and thereby to see what we can or cannot expect in a different situation where the incident electrons can penetrate liquid metals much deeper. Following the discussion in section 1, we may expect an anomalous bump in $I(\theta)$ if the condition $2\pi/q' = l$ is satisfied at some value of θ. Here, $q' = 2|k_z'|$ is the momentum transfer (in units of $\hbar$) in the interior, k_z' being given by equation (6), and l is the characteristic length of the oscillation in $\rho(z)$. We note that the momentum transfer inside the surface is given by $q' = 2|k_z'|$ rather than $q = 2k \sin\theta$ because of the refraction effect as illustrated in figure 1(a). Using equation (6), we have

$$2\pi/q' = \pi/[k^2 \sin^2\theta - 2mV_s(-\infty)/\hbar^2]^{1/2}. \tag{22}$$

For liquid In and Sn, the maximum value of $2\pi/q'$ (which occurs at $\theta = 0$) is given by $(2\pi/q')_{max} \simeq 0.75\,R_s$ and $2\pi/q' \simeq 0.42\,R_s$ at $\theta = 10$ mrad in model I, and these values are smaller than the characteristic length $l \simeq 1.5\,R_s$ of the oscillatory $\rho(z)$ in figure 2(a). These results indicate that, even if the reflection intensities due to the scattering inside the surface are sufficiently strong, the oscillatory structure of such a $\rho(z)$ produces no anomaly in the RHEED specular intensity $I(\theta)$ but reveals itself in $I(\theta)$ in an indirect manner. Nevertheless, the situtation concerning this point is not worse than that of the x-ray reflectance experiments, in which the values of $2\pi/q'$ are more than one order of magnitude larger than the characteristic length l in the range of θ where the experimental data are available (see the discussion in section 1). The scattering inside the surface becomes more important at higher θ and for higher-energy incident electrons. Therefore, possible improvements over the existing RHEED experiments should be along such a line.

(v) In model I with the use of the parametrized $\rho(z)$ given by equation (21), the monotonic $\rho(z)$ ($\delta = 0$) with $\beta_1 R_s = 6.5$ (curve A in figure 2(a)) provides a best fit (full curve in figure 2(c)) to the experimental $I(\theta)$ of liquid In. If we allow for a physically acceptable oscillation in $\rho(z)$, model I produces almost unique $I(\theta)$ in the range of small θ, which decreases too rapidly on increasing θ to explain the experimental $I(\theta)$. The theoretical results of $I(\theta)$ in model II are also almost unique in the range $\theta < 8$ mrad as we have discussed in item (ii), and these $I(\theta)$ are also too small to explain the experimental $I(\theta)$ of liquid In. These results suggest that model II, which is apparently more plausible than model I, cannot be applied to the surface of liquid In. In other words, liquid In can be treated more properly as consisting of neutral atoms in the calculations of $V_s(z)$ in the liquid–vapour transition zone. The situation of liquid Sn is quite different

from this and, as we will show in section 3.3, for this metal the predictions of model II are consistent with experiments.

3.2. Liquid In

As we have discussed in the preceding subsection, model I with the use of a monotonic atomic density profile $\rho(z)$ reproduces reasonably well the observed $I(\theta)$ and model II may be precluded in the analyses of the RHEED experiments. We also note that the behaviour of $\rho(z)$ on the vapour side, which essentially determines that part of the surface potential $V_s(z)$ in model I, is of crucial importance in determining $I(\theta)$ in the range of small θ. The parametrized $\rho(z)$ (equation (21)) used in our analyses decays exponentially on the vapour side, but such a behaviour is not realistic for classical particles as actually implied by MC simulations [2–5]. Therefore, more careful treatments of $\rho(z)$ could be essential in the analyses of the experimental $I(\theta)$ based on model I.

A realistic $\rho(z)$ would exhibit a more rapid decay than the exponential decay on the vapour side. Such a $\rho(z)$ may be obtained, though somewhat arbitrarily, from that of equation (21) by adding a term that decays linearly on the vapour side:

$$\rho(z) = \begin{cases} \rho_b[1 - B\exp(\beta_1 z)\cos(\delta z)] & (z < z_0) \\ \rho_b\{C\exp[-\beta_2(z - z_0)] - D(z - z_0)\} & (z_0 < z < z_1) \\ 0 & (z > z_1) \end{cases} \tag{23}$$

where $C = 1 - B\exp(\beta_1 z_0)\cos(\delta z_0)$ and $D(z_1 - z_0) = C\exp[-\beta_2(z_1 - z_0)]$ from the continuity conditions of $\rho(z)$ at $z = z_0$ and $z = z_1$. We also required that $d\rho(z)/dz$ is continuous at $z = z_0$ and the Gibbs dividing surface is located at $z = 0$ (see equation (20)). For oscillatory $\rho(z)$ ($\delta R_s = 4.2$), the parameter z_0 was determined by the plausible condition that z_0 is the largest (outermost) value of z at which $d^2\rho(z)/dz^2$ vanishes. This condition is reduced to

$$z_0 = (1/\delta)\tan^{-1}[(1 - \eta^2)/2\eta] \tag{24}$$

where $\eta = \delta/\beta_1$. We simply used the value $z_0 = 0$ for the monotonic $\rho(z)$ ($\delta = 0$). Five parameters can be eliminated by these requirements and we choose δ, β_1 and $d = \beta_2(z_1 - z_0)$ as the remaining parameters, where d is an important parameter determining the decay characteristic of $\rho(z)$ on the vapour side.

As before, we consider both monotonic ($\delta = 0$) and oscillatory ($\delta R_s = 4.2$) density profiles and treat β_1 and d as the fitting parameters. The density profiles $\rho(z)$ (equation (23)) that reproduce the experimental $I(\theta)$ are shown in figure 3(a) and the corresponding surface potentials $V_s(z)$ in figure 3(b). Figure 3(c) shows the comparisons of the calculated $I(\theta)$ for these $\rho(z)$. For oscillatory $\rho(z)$, $I(\theta)$ is insensitive to the damping characteristics of the oscillation (i.e. the value of β_1) in the range $\theta < 20$ mrad and the value $d = 1.0$ provides a best fit to the experimental $I(\theta)$. Therefore, in these figures only two typical cases ($\beta_1 R_s = 0.7$ and $\beta_1 R_s = 2.0$) are shown for the oscillatory $\rho(z)$. We also used the value $d = 1.0$ for the monotonic $\rho(z)$ and in this case $\beta_1 R_s = 3.4$ reproduces best the experimental $I(\theta)$, although other combinations of d and β_1 cannot be excluded. These results may be summarized as in the following.

(i) In accordance with our analyses in section 3.1, the tail part of $\rho(z)$ or $V_s(z)$ on the vapour side essentially determines the RHEED specular intensities $I(\theta)$ in the range of small θ. In fact, all the $\rho(z)$ or $V_s(z)$ that reproduce the experimental $I(\theta)$ show much

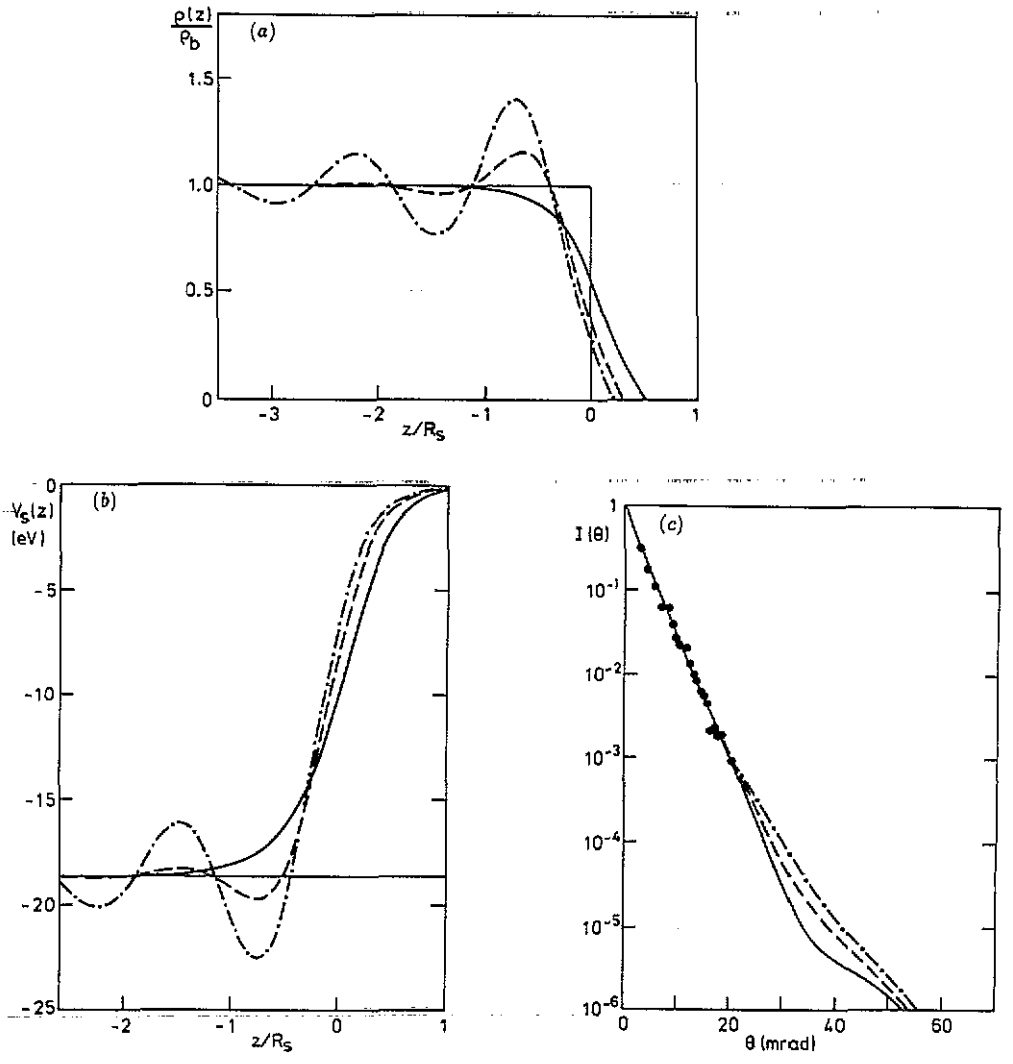

Figure 3. (*a*) Modified atomic density profiles $\rho(z)$ given by equation (23), which, with the use of model I, reproduce experimental $I(\theta)$ of liquid In: full curve, $\delta R_s = 0$ and $\beta_1 R_s = 3.4$; broken curve, $\delta R_s = 4.2$ and $\beta_1 R_s = 2.0$; chain curve, $\delta R_s = 4.2$ and $\beta_1 R_s = 0.7$. Curves in (*b*) and (*c*) show the corresponding surface potentials $V_s(z)$ (in model I) and the RHEED specular intensities $I(\theta)$ respectively. (Full curves in (*b*) and (*c*) correspond to that in (*a*) and so on.) Full circles in (*c*) show the experimental $I(\theta)$.

the same behaviour on the vapour side. We also note that the modified $\rho(z)$ given by equation (23) provides a better fit to the experimental $I(\theta)$ and therefore should be more appropriate than that given by equation (21). Unfortunately, owing to the characteristic feature of RHEED that we have discussed in section 3.1, it is difficult to determine the full behaviour of $\rho(z)$ from the existing RHEED data, which cover only the range of small θ.

(ii) The behaviours of $\rho(z)$ other than the tail part begin to influence $I(\theta)$ at $\theta \simeq 20$ mrad as demonstrated in figure 3(*c*). We find that, in the range 20 mrad $< \theta <$ 50 mrad, $I(\theta)$ is higher for larger $\rho(z)$ or deeper $V_s(z)$ just inside the tail

part (see figures 3(*a*) and (*b*)). Therefore, we need exact experimental $I(\theta)$ at higher θ for determining such behaviour of $\rho(z)$ from experiments. For such higher θ, $I(\theta)$ is too low to be measured with high accuracy at present and significant improvements in the experimental techniques would be required to obtain more detailed information on $\rho(z)$.

(iii) As we have demonstrated in the above, model I together with appropriate $\rho(z)$ provides a reasonable account of the existing RHEED experiments for liquid In. However, it does not mean that liquid In is non-metallic in the bulk but suggests only that the liquid–vapour transition zone of this metal can be described by a neutral atom model. We note that both models (model I and model II) produce similar $V_s(z)$ inside the surface and may be viewed as essentially the same as far as the bulk side is concerned.

3.3. *Liquid Sn*

As we have mentioned at the end of section 3.1, the observed RHEED specular intensity $I(\theta)$ for liquid Sn decreases much faster on increasing θ than that for liquid In (see figure 4). If we use model I and the parametrized $\rho(z)$ given by equation (21), the experimental $I(\theta)$ for liquid Sn can be reproduced best by the monotonic $\rho(z)$ with $\beta_1 R_s = 2.0$. This value of $\beta_1 R_s$ is much smaller than that of liquid In and such a highly relaxed $\rho(z)$ is not plausible near the melting point and difficult to interpret. We also note that model I with the use of a modified version of $\rho(z)$ given by equation (23) can hardly reproduce the experimental $I(\theta)$ of liquid Sn. These results suggest that model I is not applicable to the surface of liquid Sn. As we have demonstrated for liquid In, the calculated $I(\theta)$ in model II decreases much faster on increasing θ than that in model I and such a result is consistent with the observed $I(\theta)$ for liquid Sn. Therefore, it may be useful to investigate model II in more detail by applying it to liquid Sn.

As we have already discussed in section 3.1, the tail part of the surface potential $V_s(z)$ on the vapour side is essentially determined by the large relaxation of the electron density $n(z)$ at the surface and the resulting $V_s(z)$ is not sensitive to the details of the ionic density profile $\rho(z)$. For this reason, we used a parametrized $\rho(z)$ given by equation (21) in our analyses based on model II, although the above characteristic feature of model II precludes the possibilities of obtaining useful information on $\rho(z)$ from the existing RHEED experiments. Figure 4 shows the RHEED specular intensities $I(\theta)$ calculated in this way for some typical $\rho(z)$ and their comparisons with experiments. These results of $I(\theta)$ for liquid Sn actually show rapid decreases on increasing θ and are generally in reasonable agreement with experiments in the range of small θ. The insensitivity of the calculated $I(\theta)$ to $\rho(z)$ in fact makes it difficult to determine which $\rho(z)$ is most plausible, although a slightly oscillating $\rho(z)$ ($\delta R_s = 4.2$) with $\beta_1 R_s = 2.0$ (chain curve in figure 4) seems to provide a best fit to the experimental $I(\theta)$. The rapid decreases of $I(\theta)$ predicted in model II terminate at $\theta \simeq 8$ mrad and at higher θ these $I(\theta)$ show quite different behaviours depending on the steepness of $\rho(z)$ or $V_s(z)$ near the surface. Again, we need more accurate experimental $I(\theta)$ extended to higher θ for obtaining useful information on $\rho(z)$ but the prospect is much less than that for liquid In. After all, the only conclusion we can draw from our analyses of the existing RHEED data on liquid Sn is that the liquid–vapour transition zone of this metal is metallic in contrast to the case of liquid In.

4. Summary and conclusions

We have made detailed analyses on the validity of using RHEED specular intensity measurements for structural studies of liquid metal surfaces. In these analyses we ignored

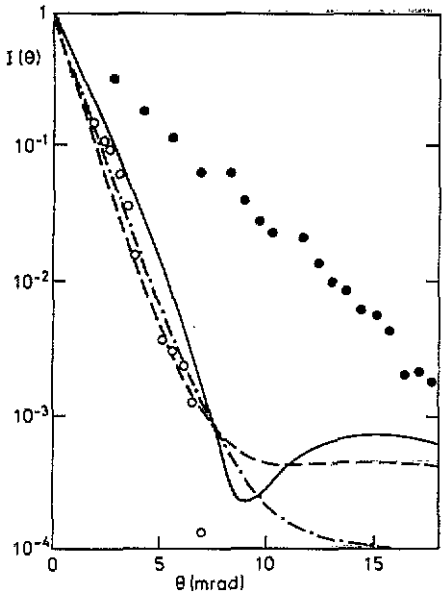

Figure 4. RHEED specular intensities $I(\theta)$ for liquid Sn calculated by using model II (curves) and their comparisons with experiments (open circles). Parameters of $\rho(z)$ (equation (21)) used in these calculations are: full curve, $\delta = 0$ and $\beta_1 R_s = 6.5$; broken curve, $\delta R_s = 4.2$ and $\beta_1 R_s = 2.0$; chain curve, $\delta R_s = 4.2$ and $\beta_1 R_s = 0.7$. Experimental $I(\theta)$ points for liquid In (full circles) are also shown for comparison. Note that the horizontal scale in this graph is expanded twice compared to that in figure 2(*c*).

the effect of inelastic scattering and used an effective refractive index model. In these basic approximations, we used two models for calculating the surface potential $V_s(z)$, which is supposed to cause the specular reflection of fast electrons: in the first model (model I) the potential felt by an external electron consists of the electrostatic potentials of neutral atoms, while in the second model (model II) liquid metals are treated as consisting of ions and extended conduction electrons.

We found that the two models produce quite different results for the RHEED specular intensity $I(\theta)$ in the range of small glancing angles θ and these different results in the two models are in parallel with the different experimental $I(\theta)$ obtained for liquid In and Sn. For liquid In, to which model I may be applicable, the tail part of the atomic density profile can be determined almost uniquely by the existing RHEED data. On the other hand, model II is plausible for liquid Sn, but in this case virtually no information can be obtained for the ionic density profile, which is masked by the distribution of the conduction electrons.

The most striking finding in our analyses may be that the liquid–vapour transition zone of liquid In is non-metallic, while liquid Sn is metallic even in that zone. This difference could be understood if the valence electrons of Sn are more loosely bound and hence more easily extended than those of In. However, theoretical predictions for such different behaviours of the conduction electrons at the liquid surface are quite difficult and may be outside the scope of the present work. Experimentally, measurements of the work function could provide other useful evidence for the different electronic structures at the surface. In fact, the electrostatic dipole potential $\varphi_{cs}(z)$ at the surface, which is the dominant contribution to the work function [13], is much reduced if the liquid–vapour transition zone becomes less metallic. Unfortunately, such experimental data are not available as far as we know.

RHEED is quite surface-sensitive because of the strong coupling between external electrons and materials and we owe the above finding about the difference between liquid In and Sn largely to this characteristic feature of RHEED. Such a difference would

not have been detected in the x-ray reflectance experiments for the reasons we have discussed in section 1. At the same time, this novel feature of RHEED makes it difficult to probe the structures inside the surface. The present analyses also suggest possible improvements over the existing RHEED experiments. One such improvement is to make exact measurements of RHEED specular intensity $I(\theta)$ at higher glancing angles, and another is to use an electron beam of higher energies. More extensive RHEED experiments are under preparation along this line and these results as well as more exact theoretical analyses are expected to appear in due course.

Acknowledgments

Part of this work was carried out under the Visiting Researcher's Program of the Institute for Materials Research, Tohoku University, through No. 880168. One of the authors (TI) would like to thank Mr H Satoh for assistance in the experiments.

References

[1] Hasegawa M 1988 *J. Phys. F: Met. Phys.* **18** 1449–71 and references therein
[2] D'Evelyn M P and Rice S A 1983 *J. Chem. Phys.* **78** 5081–95, 5225–49
[3] Gryko J and Rice S A 1984 *J. Chem. Phys.* **80** 6318–23
[4] Harris J G, Gryko J and Rice S A 1987 *J. Chem. Phys.* **87** 3069–81
[5] Ishida A, Hasegawa M and Watabe M 1990 *J. Non-Cryst. Solids* **117/118** 650–3
[6] Lu B C and Rice S A 1978 *J. Chem. Phys.* **68** 5558–67
[7] Sluis D and Rice S A 1983 *J. Chem. Phys.* **79** 5658–72
[8] Bosio L and Qumezine M 1984 *J. Chem. Phys.* **80** 959–60
[9] Hasegawa M and Ichikawa T 1990 *J. Non-Cryst. Solids* **117/118** 662–5
[10] Yoshioka H 1957 *J. Phys. Soc. Japan* **12** 618–28
[11] Radi G 1970 *Acta. Crystallogr.* A **26** 41–56 and references therein
[12] Hansen J-P and McDonald I R 1986 *Theory of Simple Liquids* 2nd edn (London: Academic)
[13] Evans R and Hasegawa M 1981 *J. Phys. C: Solid State Phys.* **14** 5225–46
[14] Hasegawa M and Watabe M 1987 *Can. J. Phys.* **65** 348–56
[15] Cohen M L and Heine V 1970 *Solid State Physics* vol 34, ed H Ehrenreich, F Seitz and D Turnbull (New York: Academic) pp 37–248
[16] Lang N D and Kohn W 1970 *Phys. Rev.* B **1** 4555–68